Human Molecular Genetics, 2012, Vol. 21, No. 20 ***4521–4529***
doi:10.1093/hmg/dds294
Advance Access published on July 23, 2012

Mitochondrial phenylalanyl-tRNA synthetase mutations underlie fatal infantile Alpers encephalopathy

Jenni M. Elo[1,†], Srujana S. Yadavalli[5,†], Liliya Euro[1], Pirjo Isohanni[1,6], Alexandra Götz[1], Christopher J. Carroll[1], Leena Valanne[7], Fowzan S. Alkuraya[9,10,11], Johanna Uusimaa[12], Anders Paetau[2] Eric M. Caruso[5], Helena Pihko[6], Michael Ibba[5], Henna Tyynismaa[1,3,*,†] and Anu Suomalainen[1,4,8,†]

[1]Research Programs Unit, Molecular Neurology, Biomedicum-Helsinki, [2]Department of Pathology, [3]Department of Medical Genetics, Haartman Institute and [4]Institute for Molecular Medicine Finland (FIMM), University of Helsinki, 00290 Helsinki, Finland, [5]Department of Microbiology and Center for RNA Biology, The Ohio State University, Columbus, OH, USA, [6]Department of Pediatric Neurology, Hospital for Children and Adolescents, [7]Medical Imaging Center and [8]Department of Neurology, Helsinki University Central Hospital, 00029 Helsinki, Finland, [9]Department of Genetics, King Faisal Specialist Hospital and Research Center and [10]Department of Pediatrics, King Khalid University Hospital, College of Medicine, King Saud University, Riyadh, Saudi Arabia and [11]Department of Anatomy and Cell Biology, College of Medicine, Alfaisal University, Riyadh, Saudi Arabia and [12]Department of Pediatrics and Clinical Research Center, Oulu University Hospital, 90220 Oulu, Finland

Received June 8, 2012; Revised July 12, 2012; Accepted July 13, 2012

Next-generation sequencing has turned out to be a powerful tool to uncover genetic basis of childhood mitochondrial disorders. We utilized whole-exome analysis and discovered novel compound heterozygous mutations in *FARS2* (mitochondrial phenylalanyl transfer RNA synthetase), encoding the mitochondrial phenylalanyl transfer RNA (tRNA) synthetase (mtPheRS) in two patients with fatal epileptic mitochondrial encephalopathy. The mutations affected highly conserved amino acids, p.I329T and p.D391V. Recently, a homozygous *FARS2* variant p.Y144C was reported in a Saudi girl with mitochondrial encephalopathy, but the pathogenic role of the variant remained open. Clinical features, including postnatal onset, catastrophic epilepsy, lactic acidemia, early lethality and neuroimaging findings of the patients with *FARS2* variants, resembled each other closely, and neuropathology was consistent with Alpers syndrome. Our structural analysis of mtPheRS predicted that p.I329T weakened ATP binding in the aminoacylation domain, and *in vitro* studies with recombinant mutant protein showed decreased affinity of this variant to ATP. Furthermore, p.D391V and p.Y144C were predicted to disrupt synthetase function by interrupting the rotation of the tRNA anticodon stem-binding domain from a closed to an open form. *In vitro* characterization indicated reduced affinity of p.D391V mutant protein to phenylalanine, whereas p.Y144C disrupted tRNA binding. The stability of p.I329T and p.D391V mutants in a refolding assay was impaired. Our results imply that the three *FARS2* mutations directly impair aminoacylation function and stability of mtPheRS, leading to a decrease in overall tRNA charging capacity. This study establishes a new genetic cause of infantile mitochondrial Alpers encephalopathy and reports a new mitochondrial aminoacyl-tRNA synthetase as a cause of mitochondrial disease.

*To whom correspondence should be addressed at: Biomedicum-Helsinki, r.C512A, Haartmaninkatu 8, 00290 Helsinki, Finland. Tel: +358 919125654; Fax: +358 919125610; Email: henna.tyynismaa@helsinki.fi
†The authors wish it to be known that, in their opinion, the first two authors should be regarded as joint First Authors and the last two authors should be regarded as joint Last Authors.

INTRODUCTION

Defects in the mitochondrial respiratory chain (RC) have been linked to an expanding group of disorders in children and adults (1). RC is composed of multi-heteromeric enzyme complexes in the mitochondrial inner membrane and is essential for cellular ATP synthesis through oxidative phosphorylation. Both nuclear genes and mitochondrial DNA (mtDNA) encode RC subunits, the mtDNA-encoded subunits being translated by mitochondrion's own translation apparatus. For this mitochondrial translation system, the ribosomal and transfer RNAs (tRNAs) are encoded by mtDNA. Maternally inherited mitochondrial tRNA mutations are a common and well-characterized cause of mitochondrial diseases. However, nuclear genes code for all ribosomal and other translation proteins for the mitochondria, including tRNA-modifying enzymes, translation elongation and termination factors, translational activators and aminoacyl-tRNA synthetases (mt-aaRSs). Defects in these proteins have increasingly been found to underlie recessively inherited mitochondrial disorders (2). Despite the essential role of mitochondrial RC in all cell types, the phenotypes of patients with mitochondrial translation defects may present as highly tissue-specific disorders and often manifest in early childhood (3).

Here, we used whole-exome sequencing to search for genetic causes underlying progressive mitochondrial encephalopathy, and report *FARS2* (mitochondrial phenylalanyl transfer RNA synthetase) mutations in mitochondrial infantile-onset encephalopathy of Alpers/Alpers–Huttenlocher type.

RESULTS

Clinical phenotype

Family 1, patient II-2 (Fig. 1), the proband, was the second child of healthy non-consanguineous parents. She was born after an uneventful pregnancy at week 41 of gestation. Her weight was 3740 g, height 51 cm, head circumference 34 cm and Apgar score 9/9. From the age of 2 days, she had myoclonic jerks, which were resistant to treatment. Her first electroencephalography (EEG) and brain magnetic resonance imaging (MRI) at the age of 4 days were normal, but at 6 weeks she had multifocal spikes in the EEG; at the age of 3 months, brain MRI showed severe central and cortical atrophy with slight bilateral signal increase in the putamina. Liver biopsy showed enlarged hepatocytes, increased amount of glycogen, lysosomal iron and copper accumulation. Her muscle biopsy sample showed weak cytochrome *c* oxidase (COX) histochemical activity, and small lipid droplets and subsarcolemmal accumulation of glycogen, but no ragged-red fibers. NADH:cytochrome *c* oxidoreductase activity was 114% of control's mean, succinate:cytochrome *c* oxidoreductase 21%, succinate dehydrogenase 50% and COX 16% of controls' mean. Plasma isoleucine, leucine and alanine were elevated and she had generalized aminoaciduria. Increased amount of lactate, up to 4.3 mmol/l, was found in the blood, and 7.2 mmol/l in cerebrospinal fluid. Blood levels of liver transaminases, creatine kinase and NH_4 were normal. MR spectroscopy at 3 months of age showed increased amount of lactate and reduction of *N*-acetylaspartate. Her cardiac function was normal. She had slightly coarse retinal pigmentation and the optic nerve looked normal. The patient's myoclonic seizures continued and she had no psychomotor development. Gastrostomy was performed at the age of 7 months. As her general condition deteriorated, active treatment was discontinued and she died at the age of 8 months.

The neuropathological autopsy revealed microcephaly, and the brain weight was 213 g (<30% of normal value). The surface of the brain showed narrowed and atrophic gyri, especially fronto-temporally (Fig. 1B). No abnormal focal lesions could be seen and the anatomical structures at the brain base were normal. The brain stem and cerebellum seemed atrophic. Microscopic examination of the frontal cortex showed striking and subtotal laminar necrosis of the whole cortical ribbon. Degeneration of the fronto-temporal cortex was almost total, with practically no remaining pyramidal cells, and the region showed mid-laminar microcystic degeneration with reactive gliosis and capillary proliferation (Fig. 1C). The hippocampi showed severe atrophy preferentially in the dentate fascia and CA4. In particular, the gyral white matter showed some presumably secondary degeneration and pallor. Basal ganglia showed neuronal degeneration with atrophy and gliosis, especially in the thalamic dorsomedial and reticular nuclei (Fig. 1D). In the brain stem, the mesencephalon was within normal range considering substantia nigra and the oculomotor complex, but some atrophy was seen in the periaqueductal grey matter. The basis of pons was quite severely atrophic and gliotic, and the medulla oblongata showed some depletion of olivocerebellar fibers in the hilar region of the inferior olives. The cerebellar cortex was quite severely atrophic with Purkinje cell drop-out, narrowed molecular and granular layers (Fig. 1E), and the dentate nucleus was moderately affected. The spinal cord and peripheral nerve showed only minor changes. The neuropathological findings were considered consistent with Alpers syndrome, and together with liver disease filled the criteria of Alpers–Huttenlocher disease.

Patient II-1, the sister of patient II-2, had died of an identical disease. Her seizures started at 4 days of age and she died of multiorgan failure at the age of 21 months after having been hospitalized for the second year of her life. She had elevated lactate values, but the histological findings of the muscle biopsy sample were normal. No autopsy was performed.

In Family 2, the index patient and her two siblings, born to consanguineous parents, have been recently described to carry a homozygous *FARS2* mutation c.431A>G (p.Y144C) (4), but the single family and lack of functional data hampered conclusions of a pathogenic role of the variant. These patients had an early-onset encephalopathy, developmental delay and uncontrolled seizures starting early in infancy. Index patient had elevated blood lactate levels and normal ammonia. Index patient expired at the age of 22 months, and her affected siblings expired before the age of 3 months.

Identification of novel *FARS2* variants by exome sequencing

MtDNA sequencing showed no pathogenic mtDNA mutations in the skeletal muscle of patient II-2, indicating recessive autosomal gene defect underlying the disorder. Exome sequencing of this patient yielded 58 685 single-nucleotide variants

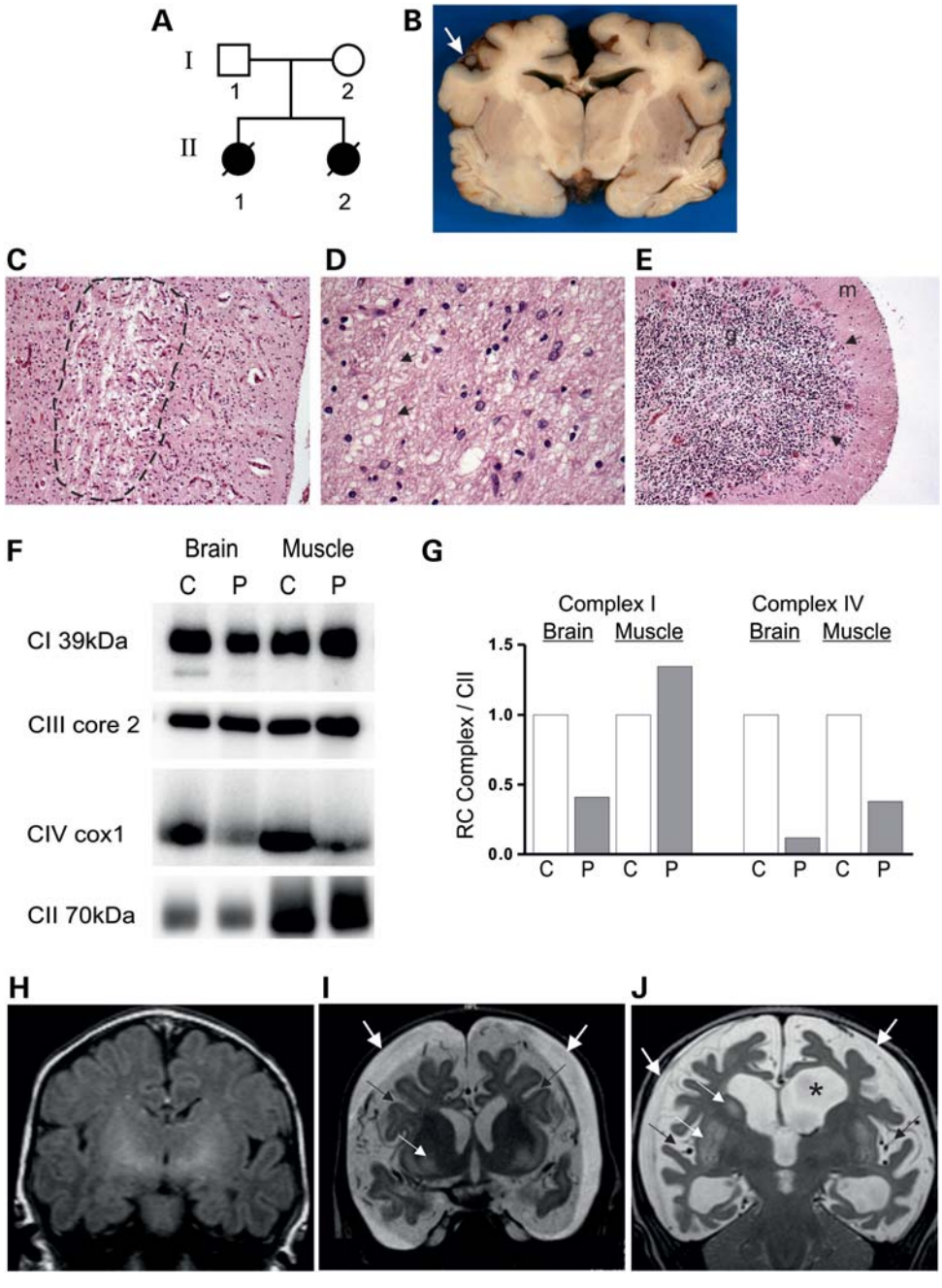

Figure 1. Patients with *FARS2* mutations. (**A**) Family 1 pedigree. (**B**) Coronal section of the brain at the level of the lenticular nucleus and anterior thalamus. The cortex of the anterior temporal lobes is especially narrow and already shows macroscopic features of laminar necrosis with cystic changes (white arrow). (**C**) In the microscopic view of the frontal cortex, practically no remaining pyramidal neurons exist, and the mid-laminar region is transformed into a microcystic track with gliosis and capillary proliferation (dotted line). HE ×200 (original magnification). (**D**) Neuronal loss, spongiosis (arrows) and gliosis can be seen in the medial/reticular thalamus. HE ×400 (original magnification). (**E**) The top of an atrophic cerebellar cortical folium shows narrowed molecular layer (m), Purkinje cell drop-out (arrows), Bergmann gliosis and a sparse granular layer (g). HE ×100 (original magnification). (**F**) Blue native electrophoresis analyses of mitochondrial RC complexes in the brain and skeletal muscle of the patient and control autopsy samples. For protein detection, monoclonal antibodies (Abcam) against the 39 kDa subunit of Complex I (CI), 70 kDa subunit of Complex II (CII), core 2 subunit of Complex III (CIII) and cox1 subunit of Complex IV (CV) were used. (**G**) Quantification of CI and CIV signal against CII from the blue native electrophoresis analyses. The result is the average of two independent blots. (**H**) Family 1, Finnish patient II-2, T1-weighted MRI scan at the age of 4 days. No cortical atrophy or abnormal findings are present. (**I**) T2-weighted image of the same patient 3 months later. Extensive brain atrophy with widened sulci (black arrows) and compensatory fluid accumulation around the cerebrum (white, thick arrows). Pathological signal change in putamen is indicated by white thin arrow. (**J**) Brain MRI of the Family 2 Saudi patient with a homozygous *FARS2* variant in exon 2 (c.A431G, p.Y144C) at 1.5 years of age, with cortical atrophy, widened sulci (black arrows) and fluid accumulation (white thick arrows). Expanded liquor space is indicated with an asterisk. White thin arrows indicate pathological signal changes in putamen (below) and nucleus caudatus (above).

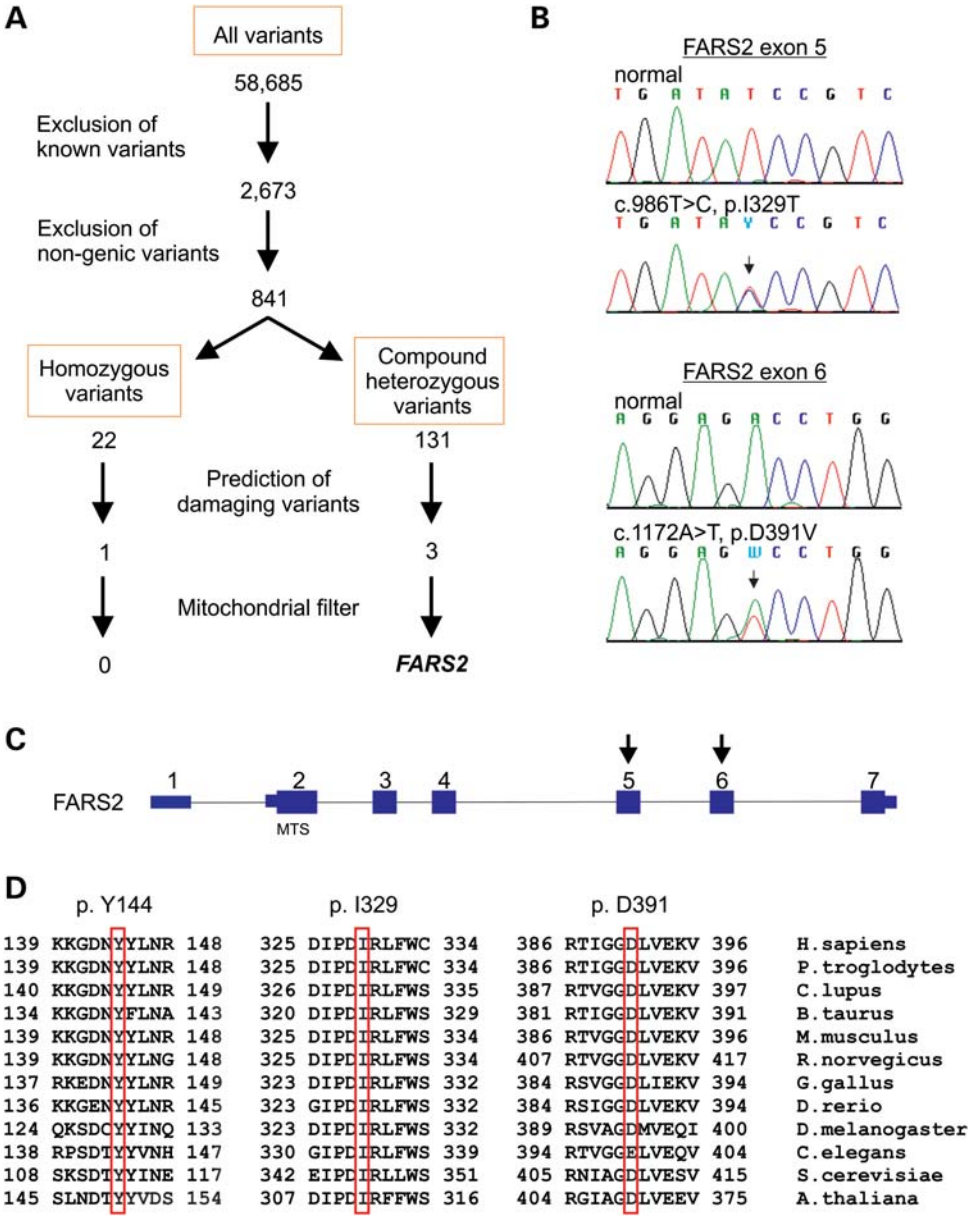

Figure 2. Identification of *FARS2* mutations. (**A**) Schematic representation of the exome data analysis and data filtering. (**B**) *FARS2* mutation sequences of exons 5 and 6. (**C**) Schematic representation of *FARS2*. Boxes represent exons 1–7. Exon 1 is non-coding. MTS denotes mitochondrial targeting signal. (**D**) Cross-species protein conservation of mtPheRS, flanking the altered amino acids p.I329, p.D391 and p.Y144 in eukaryotes.

(SNVs), which were then filtered to identify the pathogenic variants (Fig. 2A). Known dbSNP130 SNVs and non-genic variants were first excluded. Then we selected all homozygous and potentially compound heterozygous variants, and using the SIFT Genome tool, we predicted whether they were likely to be damaging for protein function. Three genes with compound heterozygous, potentially damaging variants were found, but only one of these, *FARS2*, encoded a mitochondrial-targeted protein. The identified *FARS2* variants were in exon 5, c.986T>C, p.I329T, and in exon 6, c.1172A>T, p.D391V (RefSeq NM_006567.3) (Fig. 2B). The parents were heterozygous carriers of these variants. The variants were not present in 400 Finnish control chromosomes, or in the 1000 Genomes database, and were therefore considered putative pathogenic variants.

FARS2 gene consists of seven exons, of which exons 2–7 are protein-coding (Fig. 2C). We screened these protein-coding exons and exon–intron boundaries for mutations in 82 patients with mitochondrial encephalopathy by Sanger DNA sequencing (primers are listed in Supplementary Material, Table). One patient with a rare heterozygous variant, c.1275G>C (p.L425L) and a novel heterozygous variant c.1277C>T (p.S426F) in exon 7, was identified. We tested by cDNA sequencing the potential effect of the c.1275G>C variant in splicing, but both alleles of *FARS2* were equally present in fibroblast cDNA. This patient also carried a

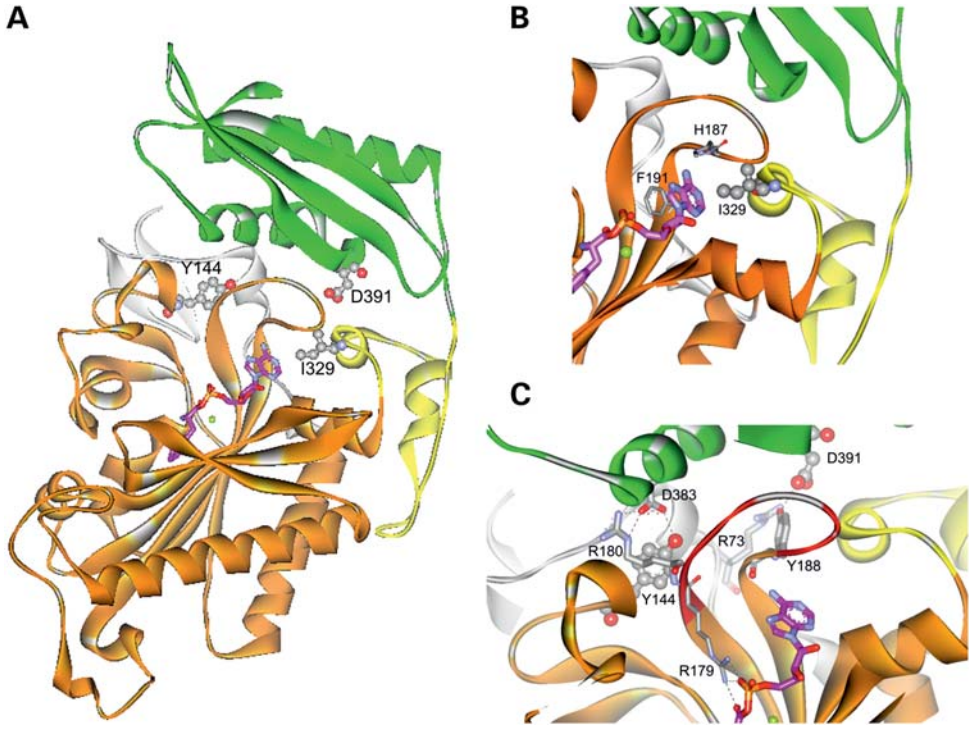

Figure 3. Structure of mtPheRS. (**A**) Location of Ile329, Asp391 and Tyr144 within the resolved structure of human mtPheRS (PDB id 3CMQ). The catalytic domain is in orange, the linker is in yellow and the anticodon-binding domain is in green. Carbon atoms of phenylalanyl-adenylate are in magenta, magnesium atom is represented as green sphere. (**B**) Location of Ile329 within the aminoacylation domain of mtPheRS. Ile329 is represented in ball-and-stick model. Residues interacting with ATP are shown. Phe191 forming stacking interaction with adenyl ring of ATP is marked. (**C**) Contacts formed by Asp391 and Tyr144 with neighboring residues in the interface between two domains. The loop-encompassing residues Arg179-His187 is in red. Hydrogen bonds are represented as black dashed lines. Color code for the domains as in (A).

known SNV leading to the p.N280S amino acid change, which previously has been shown to affect protein refolding (5). However, this SNV has an allele frequency of 0.15 in Europeans (1000 Genomes), and was not considered to be a likely disease mutation.

RC analyses and mitochondrial translation

FARS2 encodes the mitochondrial phenylalanyl-tRNA synthetase (mtPheRS), which is responsible for the charging of $tRNA^{Phe}$ with phenylalanine in mitochondrial translation. Defects in mtPheRS activity are thus expected to disrupt the synthesis of mtDNA-encoded RC proteins. Blue native electrophoresis (BN-PAGE, Blue native polyacrylamide gel electrophoresis) of the mitochondrial RC complexes revealed a severe reduction of COX (Complex IV) in the brain and skeletal muscle and partial Complex I deficiency in the brain (Fig. 1F and G). However, patients' fibroblasts did not display decreased mitochondrial translation or reduction in the number of RC complexes (data not shown), hindering the use of cultured patient cells in functional studies. Similar lack of phenotype in cultured cells has been observed in many other mt-aaRS defects (6,7), with the exception of mitochondrial methionyl-tRNA synthetase 2 (*MARS2*) defects manifesting in lymphoblasts and *YARS2* (mitochondrial tyrosyl-tRNA synthetase 2) defects in myotubes and myoblasts (8–10).

Neuroimaging findings of patients

Next we compared the neuroimaging findings of the Finnish and Saudi patients, as diseases caused by mt-aaRS defects often show gene-specific brain MRI patterns (7,11). At the age of 4 days, patient II-2 from Family 1 had normal brain MRI (Fig. 1H), but at the age of 3 months had developed severe brain atrophy with compensatory subdural fluid accumulation around the cerebrum, and pathological signal intensities in both putamina (Fig. 1I). The Saudi patient had very similar brain MRI findings to the Finnish patient at the age of 1.5 years, showing extensive cerebral atrophy with subdural fluid accumulation, and pathological bilateral signal intensities in the putamina (Fig. 1J). This patient also showed signal changes in both caudate nuclei. Both patients had relative sparing of the cerebellum.

Structural modeling of the mutations affecting mtPheRS

The mtPheRS amino acids altered in the Finnish patients, Ile329 and Asp391, and in the Saudi patient, Tyr144, are all highly conserved residues among eukaryotes (Fig. 2D). Examination of the crystal structure of human mtPheRS (12) shows Ile329 as part of the ATP-binding site in the aminoacylation domain, whereas Asp391 is in the anticodon stem-binding domain (Fig. 3A). We predicted that the change of Ile329 for the small, uncharged, threonine would result in a widened ATP-binding site, leading to decreased affinity for

ATP (Fig. 3B). Structural and biochemical studies have shown that mtPheRS exists in a dynamic equilibrium between the closed and open conformational states, and tRNA-binding stabilizes the open form (12–14). Binding of tRNA is thought to trigger rotation of the anticodon-binding domain away from the aminoacylation domain to the position optimal for interaction with the anticodon loop of tRNA. Asp391 is one of the residues on the contact surface between the aminoacylation and anticodon-binding domains. It is involved in the stabilization of the closed form of the enzyme by forming hydrogen bonds with Arg73 and Tyr188 (Fig. 3C). We predicted that the change of Asp391 to valine would alter the rotation mechanism upon tRNA binding, thus affecting the conformational flexibility of the enzyme. The Tyr144 altered in the Saudi patient (4) locates in the mtPheRS aminoacylation domain on the interface of the anticodon stem-binding domain, and participates in the stabilization of the closed structure by forming hydrogen bonds with Arg180 and Asp383 (Fig. 3C). Consequences of the p.Y144C change for the synthetase function are thus likely to be similar to p.D391V. These structural data predict a pathogenic role for all the three identified *FARS2* mutations.

Functional analysis of recombinant mutant mtPheRS

To test the functional effects of the *FARS2* mutations *in vitro*, we expressed and purified the recombinant mutant mtPheRS proteins in *Escherichia coli*, according to previously published procedures (14). ATP-PP_i exchange kinetic assays for amino acid activation revealed a significant difference in ATP binding between the wild-type and p.I329T mtPheRS, supporting the structural prediction of a widened ATP-binding site in the mutant. The p.I329T replacement led to a ~4-fold decrease in the catalytic efficiency of amino acid activation due to a 2.5-fold increase in K_M for ATP, as predicted by the structural modeling, and a small decrease in k_{cat} (Table 1). Phe binding was essentially unaffected in the p.I329T mutant, but interestingly, we observed that the p.D391V replacement, which is distal from the active site, led to an increase in K_M for Phe (Table 2). Therefore, *in vivo*, under limited substrate availability, the p.D391V mutation may significantly decrease mtPheRS aminoacylation activity. ATP- or Phe-binding were not affected by the p.Y144C replacement. Steady-state charging assays were also performed to determine the effect of mutations on $tRNA^{Phe}$ binding. Both the p.I329T and p.D391V mtPheRS variants showed only modest changes in their catalytic efficiencies for $tRNA^{Phe}$ charging, whereas p.Y144C mutant had a clearly increased K_M for tRNA (Table 3).

In addition to the direct impact on function, we analyzed the effect of p.I329T and p.D391V amino acid replacements on the stability of mtPheRS by refolding assay. Our results show that the single mutants p.I329T and p.D391V refold only to ~35–45% of the original active fraction, whereas the WT retains almost 80–90% of its active folded form (Fig. 4). Therefore, the p.I329T and p.D391V substitutions in mtPheRS not only impair aminoacylation function directly by perturbing small molecule binding in the active site, but also affect the stability of mtPheRS, leading to a significant decrease in overall charging capacity. These results experimentally verified the effects of the mutations on catalytic activity, and strongly support a pathogenic role of all identified *FARS2* mutations.

Table 1. Steady-state PP_i exchange kinetic constants for ATP with wild-type and mutant mtPheRSs

mtPheRS	k_{cat}^{ATP} (s^{-1})	K_M^{ATP} (mM)	k_{cat}/K_M (s^{-1} mM^{-1})
WT	7.4 ± 0.3	2.9 ± 0.3	2.5 ± 0.3
I329T	5 ± 0.1	7.3 ± 0.9	0.7 ± 0.1
D391V	5.6 ± 0.1	2.5 ± 0.04	2.2 ± 0.02
Y144C	5.7 ± 0.3	2.3 ± 0.01	2.5 ± 0.1

ATP was varied in the range of 1–25 mM. Enzyme concentrations were normalized by active site titration. Data represent averages and standard errors from three independent trials.

Table 2. Steady-state PP_i exchange kinetic constants for Phe with wild-type and mutant mtPheRSs

mtPheRS	k_{cat}^{Phe} (s^{-1})	K_M^{Phe} (μM)	k_{cat}/K_M (s^{-1} μM^{-1})
WT	1.7 ± 0.1	7.3 ± 0.5	0.2 ± 0.01
I329T	1.6 ± 0.2	8.6 ± 1.7	0.2 ± 0.02
D391V	2.3 ± 0.02	20.9 ± 1.2	0.1 ± 0.01
Y144C	1.4 ± 0.2	7.5 ± 1.4	0.2 ± 0.02

Phe was varied in the range of 5–800 μM. Enzyme concentrations were normalized by active-site titration. Data represent averages and standard errors from three independent trials.

Table 3. Steady-state aminoacylation kinetic constants for $tRNA^{Phe}$ with wild-type and mutant mtPheRSs

mtPheRS	k_{cat}^{tRNA} (s^{-1})	K_M^{tRNA} (μM)	k_{cat}/K_M (s^{-1} μM^{-1})
WT	0.09 ± 0.01	1.2 ± 0.2	0.07 ± 0.01
I329T	0.05 ± 0.005	1.2 ± 0.4	0.05 ± 0.01
D391V	0.07 ± 0.01	1.4 ± 0.2	0.05 ± 0.01
Y144C	0.06 ± 0.02	2.8 ± 0.3	0.02 ± 0.01

Human mitochondrial $tRNA^{Phe}$ was varied in the range of 0.05–4 μM. Kinetic parameters were estimated using sub-saturating concentrations of $tRNA^{Phe}$. Enzyme concentrations were normalized by active-site titration. Data represent averages and standard errors from at least three independent trials. k_{cat}/K_M was estimated directly from the slope of the equation, $V = k_{cat}[E][S]/K_M$, where [E] = enzyme concentration, [S] = substrate concentration.

DISCUSSION

Here, we provide evidence that *FARS2* mutations lead to mitochondrial encephalopathy with neonatal disease-onset, treatment-resistant epilepsy, lactacidosis and developmental arrest. The neuroimaging findings were highly similar between the Finnish and Saudi patients, including severe progressive cerebral atrophy. The neuropathological findings were consistent with Alpers syndrome, previously only associated with mutations of mtDNA polymerase γ (*POLG*, MIM 174763) (15) and helicase Twinkle (*C10ORF2*, MIM 606075) (16). We proved the pathological potential of the identified *FARS2* mutations by protein modeling and by

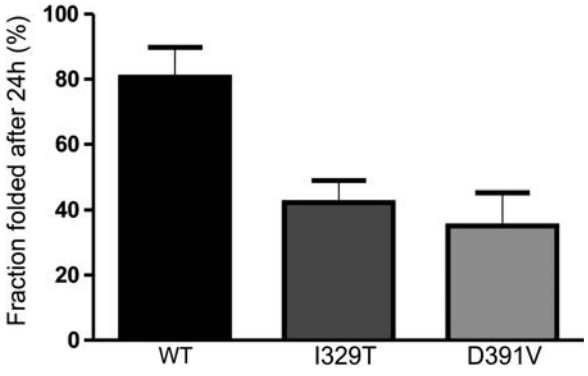

Figure 4. Aminoacylation and the stability of mtPheRS. The stability of the mutant mtPheRS was tested by determining the active fraction of the mutant and wild-type mtPheRSs by active site titration, followed by incubation at room temperature for 24 h and re-measured activity to quantify the properly folded fraction.

biochemical and functional characterization of recombinant proteins, and showed that they lead to defective tRNA aminoacylation and tissue-specific mitochondrial RC deficiency.

The shared known function of mt-aaRSs is to specifically recognize and bind to their cognate mitochondrial tRNAs and catalyze the transfer of the appropriate amino acid to the acceptor stem of the tRNA, thereby being essential for mitochondrial translation. However, the clinical variability and tissue specificity of the associated disorders are remarkable. *DARS2* (mitochondrial aspartyl-tRNA synthetase 2) mutations lead to leukoencephalopathy with brain stem and spinal cord involvement and lactate elevation (LBSL, MIM 611105) (7). *RARS2* (mitochondrial arginyl-tRNA synthetase 2) mutations cause pontocerebellar hypoplasia type 6 (MIM 611523) (17), whereas *YARS2* defects underlie myopathy, lactic acidosis and sideroblastic anemia (MLASA, MIM 613561) (9). Perrault syndrome with ovarian dysgenesis in females and sensorineural hearing loss in males and females have been reported to be caused by *HARS2* (mitochondrial histidyl-tRNA synthetase 2) mutations (MIM 600783) (18), and the HUPRA (hyperuricemia, pulmonary hypertension, renal failure in infancy and alkalosis) syndrome in infancy by *SARS2* mutations (MIM 612804). We previously identified *AARS2* mutations in infantile cardiomyopathy patients (MIM 612035) (6). Recently, *MARS2* mutations were reported in spastic ataxia with leukoencephalopathy (ARSAL, MIM 609728) (8), and *EARS2* mutations in leukoencephalopathy with thalamus and brainstem involvement and high lactate (LTBL, MIM 621799) (11). Our current study establishes *FARS2* as a disease gene for early-childhood fatal mitochondrial encephalopathy. The molecular basis of this exceptional variability in disease manifestations remains to be solved.

Tissue specificity and genotype–phenotype correlation of mt-aaRS disorders is expressed both in clinical and neuroimaging findings (7,11). The LBSL patients with *DARS2* mutations have a uniform diagnostic brain MRI pattern comprising of signal abnormalities in the cerebral white matter and specific brain stem and spinal cord tracts (7). Patients with *EARS2* mutations display a distinct but also diagnostic brain MRI pattern with extensive symmetrical cerebral white matter abnormalities sparing the periventricular rim and symmetrical signal abnormalities of the thalami, mid-brain, pons, medulla oblongata and cerebellar white matter (11). The two patients with the different *FARS2* mutations described in this study shared highly similar MRI findings showing extensive cerebral atrophy with subdural fluid accumulation, and bilateral putaminal pathological signal intensities. The reason for the differential specificity of the mitochondrial aminoacyl-tRNA synthetase defects of the brain is unknown.

The neuropathological findings of the Finnish *FARS2* patient, with laminar cortical necrosis and severe cortical atrophy, were consistent with the diagnosis of Alpers disease (19,20). Alpers disease has been associated with recessive mutations in *POLG* and *C10ORF2* (15,16,20), but many patients with typical signs do not have mutations in these genes. Alpers–Huttenlocher disorder typically shows brain and liver involvement (21). The Finnish *FARS2* patient had pathological liver histology. The Saudi patient, however, with similar brain MRI as the Finnish patients, showed no signs of liver disease. Alpers syndrome patients with *POLG* mutations commonly develop valproate toxicity-induced liver dysfunction after epilepsy treatment (22). In the Finnish *FARS2* patients, the liver dysfunction existed before valproate treatment, suggesting no similar valproate sensitivity as in *POLG*-Alpers. Our findings suggest that *FARS2* mutations are a new cause of Alpers encephalopathy, which may manifest with or without liver dysfunction.

mtPheRS consists of 451 amino acids, of which 37 N-terminal residues form the mitochondrial targeting signal (23). The synthetase has a catalytic aminoacylation domain (residues 84–325) and a C-terminal anticodon stem-binding domain (residues 359–451) separated by a linker (residues 326–358). MtPheRS, a monomer, is unusual among phenylalanyl-tRNA synthetases, as bacterial and eukaryotic cytoplasmic synthetases are heterotetramers consisting of two α-subunits and two β-subunits (23). An mtPheRS monomer contains an aminoacylation domain, homologous to the bacterial α-subunit and an anticodon-binding domain, homologous to the C-terminus of the bacterial β-subunit. It also lacks the structural module, present in bacterial and eukaryotic cytosolic PheRSs, responsible for proofreading a non-cognate tyrosine (24,25). mtPheRS has two functional conformations. In its open form, it binds tRNA and catalyzes the attachment of Phe to its cognate tRNA in the aminoacylation domain. The closed form has the anticodon stem-binding domain rotated back close to the aminoacylation domain. By measuring the steady-state kinetics of the recombinant mutant proteins, we identified three alternative ways, by which the mutations affected the aminoacylation efficiency of the synthetase. First, we predicted the p.I329T mutant to widen the ATP-binding pocket, and found decreased ATP binding by the recombinant mutant protein, whereas phenylalanine and tRNA binding were unaffected. The amino acid changes p.D391V and p.Y144C are located at the interface between the aminoacylation and anticodon-binding domains. We hypothesized that these mutations would interfere with the rotation mechanism of the synthetase, which could affect the tRNA binding. This was found to be true for the p.Y144C mutant. On the contrary, we observed that, *in vitro*, the p.D391V mutant had normal K_M for ATP and tRNA, but a significantly decreased affinity for phenylalanine.

To explain why Asp391, which is not situated at the active site, had decreased phenylalanine binding, we propose the following. Asp391 is involved in a close network of interactions with the conserved residue Arg330 near motif 3 (which is adjacent to Ile329), Tyr188 in motif 2 and Arg73. The p.D391V replacement may cause Arg330 and other neighboring residues to adopt different conformations, leading to perturbation in the loop encompassing residues Arg179-His187, of which Arg179 is critical for binding and coordination of phenylalanine (Fig. 3C). In addition, the overall stability of the tested mutants was compromised. Thus, the mutations affected both the function and the stability of mtPheRS, impairing its tRNA charging capacity.

In conclusion, we provide clinical, genetic, structural and functional evidence that *FARS2* mutations are a novel cause of mitochondrial translation disorder, leading to neonatal onset progressive Alpers syndrome.

MATERIALS AND METHODS

Patient studies

Patient samples for the study were taken according to the Declaration of Helsinki, with informed consent given prior to sample collection. The ethical review board of the Helsinki University Central Hospital approved the study.

RC enzyme activities were determined as previously described (26). The activities were calculated as ratios to citrate synthase activity. Blue native electrophoresis (BN-PAGE) of the mitochondrial RC complexes (27) and mtDNA sequencing (6) were performed as previously described.

Exome sequencing

Exome targets were enriched from patient's total DNA, using the NimbleGen Sequence Capture 2.1 M Human Exome v1.0 array, followed by sequencing with the Illumina Genome Analyzer-IIx platform. The variant-calling pipeline of the Finnish Institute for Molecular Medicine was used for the reference genome alignment and variant calling (28). As a result, 94.86% of target coverage was reached, with 20-fold coverage for 53.23% of targets. This approach yielded 58 685 SNVs, which were then filtered to identify the pathogenic variants.

Functional assays

E. coli strain BL21 (pArgU218)/pET21c-PheRS expressing C-terminal His_6-tagged mtPheRS was a gift from Prof. Linda Spremulli (University of North Carolina, Chapel Hill, NC, USA). Point mutations were introduced by site-directed mutagenesis using the QuikChange procedure (Stratagene). *In vitro* aminoacylation assays were performed at 37°C in aminoacylation buffer containing 100 mM Na-Hepes (pH 7.2), 30 mM KCl, 2 mM ATP, 10 mM $MgCl_2$. Reaction mixture contained 40 μM L-[^{14}C]Phe (215 cpm/pmol, Perkin Elmer Lifesciences), 2.5 μM native *E. coli* $tRNA^{Phe}$ and 100 nM hmtPheRS. Nine microliters of aliquots were removed and spotted on 3 mm filter disks (Whatman), washed three times in 10% trichloroacetic acid and dried. The amount of radioactivity retained was determined by liquid scintillation counting. Steady-state kinetics were investigated at 37°C as previously described (24,29). For ATP-PP_i exchange kinetics for amino acid activation, concentrations of substrates were varied from 5–800 μM for Phe and 1–25 mM for ATP. Enzymes were added to a final concentration of 100–150 nM. In the steady-state charging assays, the concentrations of mitochondrial $tRNA^{Phe}$ varied between 0.05 and 4 μM and enzymes were added to a final concentration of 50 nM.

For protein refolding, active fractions of 1–5 μM of all the protein samples were incubated in aminoacylation buffer. After 24 h, amino acid activation was performed. Active site titration was done in a 50 μl of reaction mixture containing 100 mM Na–Hepes, pH 7.2, 30 mM KCl, 10 mM $MgCl_2$, 2 mM ATP, 25 μM L-[^{14}C]Phe (215 cpm/pmol) and 5 mM β-mercaptoethanol and 2 U/ml inorganic pyrophosphatase. The reaction was initiated by the addition of mtPheRS to reaction mixture pre-incubated at 37°C for 5 min. After adding the enzyme, the reaction was performed for 10 min at 37°C and then filtered through a nitrocellulose membrane (Whatman PROTRAN BA85) pre-washed with cold 0.5× aminoacylation buffer. The filters were then washed with 3 ml of cold 0.5× aminoacylation buffer and dried at 85°C for 30 min. The amount of radioactivity retained was quantified by liquid scintillation counting. Data from at least three independent experiments were averaged and resulting standard errors are shown.

SUPPLEMENTARY MATERIAL

Supplementary Material is available at *HMG* online.

ACKNOWLEDGEMENTS

Ilse Paetau, Sofia Ahola-Erkkilä, Joni Nikkanen, Rosanna Pöyhönen and Sanna Matilainen are thanked for technical help. We also acknowledge the exome capture, sequencing and variant-calling pipeline analyses performed by the Institute for Molecular Medicine Finland FIMM, Technology Centre and University of Helsinki.

*Conflict of Interest*statement. None declared.

FUNDING

This work was supported by Jane and Aatos Erkko Foundation (to A.S.); Sigrid Jusélius Foundation; Academy of Finland and University of Helsinki (to A.S. and H.T.); Helsinki Biomedical Graduate School (to J.M.E.); Arvo and Lea Ylppö Foundation and Orion Farmos Research Foundation (to H.T.); and the National Science Foundation (to M.I.).

REFERENCES

1. Ylikallio, E. and Suomalainen, A. (2011) Mechanisms of mitochondrial diseases. *Ann. Med.*, **44**, 41–59.
2. Rotig, A. (2011) Human diseases with impaired mitochondrial protein synthesis. *Biochim. Biophys. Acta*, **1807**, 1198–1205.
3. Uziel, G., Ghezzi, D. and Zeviani, M. (2011) Infantile mitochondrial encephalopathy. *Semin. Fetal Neonatal Med.*, **16**, 205–215.

4. Shamseldin, H.E., Alshammari, M., Al-Sheddi, T., Salih, M.A., Alkhalidi, H., Kentab, A., Repetto, G.M., Hashem, M. and Alkuraya, F.S. (2012) Genomic analysis of mitochondrial diseases in a consanguineous population reveals novel candidate disease genes. *J. Med. Genet.*, **49**, 234–241.
5. Banerjee, R., Reynolds, N.M., Yadavalli, S.S., Rice, C., Roy, H., Banerjee, P., Alexander, R.W. and Ibba, M. (2011) Mitochondrial aminoacyl-tRNA synthetase single-nucleotide polymorphisms that lead to defects in refolding but not aminoacylation. *J. Mol. Biol.*, **410**, 280–293.
6. Götz, A., Tyynismaa, H., Euro, L., Ellonen, P., Hyotylainen, T., Ojala, T., Hamalainen, R.H., Tommiska, J., Raivio, T., Oresic, M. *et al.* (2011) Exome sequencing identifies mitochondrial alanyl-tRNA synthetase mutations in infantile mitochondrial cardiomyopathy. *Am. J. Hum. Genet.*, **88**, 635–642.
7. Scheper, G.C., van der Klok, T., van Andel, R.J., van Berkel, C.G., Sissler, M., Smet, J., Muravina, T.I., Serkov, S.V., Uziel, G., Bugiani, M. *et al.* (2007) Mitochondrial aspartyl-tRNA synthetase deficiency causes leukoencephalopathy with brain stem and spinal cord involvement and lactate elevation. *Nat. Genet.*, **39**, 534–539.
8. Bayat, V., Thiffault, I., Jaiswal, M., Tetreault, M., Donti, T., Sasarman, F., Bernard, G., Demers-Lamarche, J., Dicaire, M.J., Mathieu, J. *et al.* (2012) Mutations in the mitochondrial methionyl-tRNA synthetase cause a neurodegenerative phenotype in flies and a recessive ataxia (ARSAL) in Humans. *PLoS Biol.*, **10**, e1001288.
9. Riley, L.G., Cooper, S., Hickey, P., Rudinger-Thirion, J., McKenzie, M., Compton, A., Lim, S.C., Thorburn, D., Ryan, M.T., Giege, R. *et al.* (2010) Mutation of the mitochondrial tyrosyl-tRNA synthetase gene, YARS2, causes myopathy, lactic acidosis, and sideroblastic anemia—MLASA syndrome. *Am. J. Hum. Genet.*, **87**, 52–59.
10. Sasarman, F., Nishimura, T., Thiffault, I. and Shoubridge, E.A. (1012) A novel mutation in YARS2 causes myopathy with lactic acidosis and sideroblastic anemia. *Hum. Mutat.* 10.1002/humu.22098.
11. Steenweg, M.E., Ghezzi, D., Haack, T., Abbink, T.E., Martinelli, D., van Berkel, C.G., Bley, A., Diogo, L., Grillo, E., Te Water Naude, J. *et al.* (2012) Leukoencephalopathy with thalamus and brainstem involvement and high lactate 'LTBL' caused by EARS2 mutations. *Brain*, **135**, 1387–1394.
12. Klipcan, L., Levin, I., Kessler, N., Moor, N., Finarov, I. and Safro, M. (2008) The tRNA-induced conformational activation of human mitochondrial phenylalanyl-tRNA synthetase. *Structure*, **16**, 1095–1104.
13. Klipcan, L., Moor, N., Finarov, I., Kessler, N., Sukhanova, M. and Safro, M.G. (2011) Crystal structure of human mitochondrial PheRS complexed with tRNA(Phe) in the active 'open' state. *J. Mol. Biol.*, **415**, 527–537.
14. Yadavalli, S.S., Klipcan, L., Zozulya, A., Banerjee, R., Svergun, D., Safro, M. and Ibba, M. (2009) Large-scale movement of functional domains facilitates aminoacylation by human mitochondrial phenylalanyl-tRNA synthetase. *FEBS Lett.*, **583**, 3204–3208.
15. Naviaux, R.K., Nyhan, W.L., Barshop, B.A., Poulton, J., Markusic, D., Karpinski, N.C. and Haas, R.H. (1999) Mitochondrial DNA polymerase gamma deficiency and mtDNA depletion in a child with Alpers' syndrome. *Ann. Neurol.*, **45**, 54–58.
16. Hakonen, A.H., Isohanni, P., Paetau, A., Herva, R., Suomalainen, A. and Lonnqvist, T. (2007) Recessive Twinkle mutations in early onset encephalopathy with mtDNA depletion. *Brain*, **130**, 3032–3040.
17. Edvardson, S., Shaag, A., Kolesnikova, O., Gomori, J.M., Tarassov, I., Einbinder, T., Saada, A. and Elpeleg, O. (2007) Deleterious mutation in the mitochondrial arginyl-transfer RNA synthetase gene is associated with pontocerebellar hypoplasia. *Am. J. Hum. Genet.*, **81**, 857–862.
18. Pierce, S.B., Chisholm, K.M., Lynch, E.D., Lee, M.K., Walsh, T., Opitz, J.M., Li, W., Klevit, R.E. and King, M.C. (2011) Mutations in mitochondrial histidyl tRNA synthetase HARS2 cause ovarian dysgenesis and sensorineural hearing loss of Perrault syndrome. *Proc. Natl Acad. Sci. USA*, **108**, 6543–6548.
19. Alpers, B.J. (1931) Diffuse progressive degeneration of the grey matter of the cerebrum. *Arch. Neurol. Psychiatry*, **25**, 469–505.
20. Naviaux, R.K. and Nguyen, K.V. (2004) POLG mutations associated with Alpers' syndrome and mitochondrial DNA depletion. *Ann. Neurol.*, **55**, 706–712.
21. Huttenlocher, P.R., Solitare, G.B. and Adams, G. (1976) Infantile diffuse cerebral degeneration with hepatic cirrhosis. *Arch. Neurol.*, **33**, 186–192.
22. Van Goethem, G., Luoma, P., Rantamaki, M., Al Memar, A., Kaakkola, S., Hackman, P., Krahe, R., Lofgren, A., Martin, J.J., De Jonghe, P. *et al.* (2004) POLG mutations in neurodegenerative disorders with ataxia but no muscle involvement. *Neurology*, **63**, 1251–1257.
23. Bullard, J.M., Cai, Y.C., Demeler, B. and Spremulli, L.L. (1999) Expression and characterization of a human mitochondrial phenylalanyl-tRNA synthetase. *J. Mol. Biol.*, **288**, 567–577.
24. Roy, H., Ling, J., Alfonzo, J. and Ibba, M. (2005) Loss of editing activity during the evolution of mitochondrial phenylalanyl-tRNA synthetase. *J. Biol. Chem.*, **280**, 38186–38192.
25. Ling, J., Roy, H. and Ibba, M. (2007) Mechanism of tRNA-dependent editing in translational quality control. *Proc. Natl Acad. Sci. USA*, **104**, 72–77.
26. Majander, A., Rapola, J., Sariola, H., Suomalainen, A., Pohjavuori, M. and Pihko, H. (1995) Diagnosis of fatal infantile defects of the mitochondrial respiratory chain: age dependence and postmortem analysis of enzyme activities. *J. Neurol. Sci.*, **134**, 95–102.
27. Wittig, I., Braun, H.P. and Schagger, H. (2006) Blue native PAGE. *Nat. Protoc.*, **1**, 418–428.
28. Sulonen, A.M., Ellonen, P., Almusa, H., Lepisto, M., Eldfors, S., Hannula, S., Miettinen, T., Tyynismaa, H., Salo, P., Heckman, C. *et al.* (2011) Comparison of solution-based exome capture methods for next generation sequencing. *Genome Biol.*, **12**, R94.
29. Roy, H., Ling, J., Irnov, M. and Ibba, M. (2004) Post-transfer editing in vitro and in vivo by the beta subunit of phenylalanyl-tRNA synthetase. *EMBO J.*, **23**, 4639–4648.